nature electronics

REVIEW ARTICLE

https://doi.org/10.1038/s41928-020-0390-3

Electronic neural interfaces

Milin Zhang[1]✉, Zijian Tang[1], Xilin Liu[2] and Jan Van der Spiegel[2]

Devices such as keyboards and touchscreens allow humans to communicate with machines. Neural interfaces, which can provide a direct, electrical bridge between analogue nervous systems and digital man-made systems, could provide a more efficient route to future information exchange. Here we review the development of electronic neural interfaces. The interfaces typically consist of three modules — a tissue interface, a sensing interface, and a neural signal processing unit — and based on technical milestones in the development of the electronic sensing interface, we group and analyse the interfaces in four generations: the patch clamp technique, multi-channel neural interfaces, implantable/wearable neural interfaces and integrated neural interfaces. We also consider key circuit and system challenges in the design of neural interfaces and explore the opportunities that arise with the latest technology

Since the creation of the transistor in 1947, a variety of devices have been developed that can provide a communication channel between humans and the digital world. These devices, which include keyboards, mice and touchscreens, communicate effectively with a digital system by translating user movements and reflecting user intent. This intent originates from the human nervous system and thus an ultimate goal of such communication is to bypass these devices and establish a direct communication channel between user intent (that is, neural signals) and the digital word. Due to advanced silicon electronics, this is now possible using neural interfaces or brain–machine interfaces.

A neural interface builds a bidirectional communication channel between a subject's nervous system and a man-made device. A typical interface consists of three key modules (Fig. 1a): a tissue interface, a electronic sensing interface, and a neural signal processing unit. Based on technical milestones in the development of the electronic sensing interface, neural interfaces can be roughly divided into four generations (Fig. 1b). The first generation — the patch clamp — enabled in vitro neural signal acquisition, but required complex procedures to prepare the biosamples before the neural signals could be measured. The second generation — multi-channel neural interfaces — enabled in vivo experiments, but the types of experiments that could be conducted were limited by the cable used to connect the in vivo electrodes and the workstation for data acquisition, signal processing and control. The third generation — implantable/wearable neural interfaces — integrated the neural signal acquisition with wireless communication, and enabled long-term operation in freely moving subjects. Some devices included only a wireless transmission unit, whereas more advanced devices included signal processing functions, making them self-contained. However, the electrodes were still separated from the sensing module, causing size overhead and tissue damage. The fourth generation — integrated neural interfaces — integrated the electrodes together with the electronic sensing interface consisting of low-power amplifiers and filters, and more recently, even the signal processing unit, onto the same substrate. This has led to ultracompact structures with low-power and high-density electrode capabilities.

In this Review Article, we trace the development of electronic neural interfaces through the four generations of technology, and consider the challenges and opportunities that arise with the latest devices.

The patch clamp technique

Key to the development of electronic neural interfaces is electrophysiology, which studies the electrical properties of cells and tissues. The exploration of electrophysiology can be traced back to the 18th century, when Luigi Galvani applied charges to the nerves of dead frogs' muscles using a Leyden jar and observed contractions of the muscles[1]. It was though in the middle of the 20th century that crucial capabilities began to emerge.

In 1949, voltage clamp technology was invented[2], which allowed Alan Hodgkin and Andrew Huxley to record currents carried by sodium and potassium ions through nerve cell membranes using electrochemical gradients[3]. The Hodgkin–Huxley model was then introduced in 1952 to mathematically describe the membrane potentials using a resistor–capacitor (RC) circuit model[4] (Fig. 2a). Later, in 1976, Erwin Neher and Bert Sakmann developed the patch clamp technique to record single ion channel signals (Fig. 2b,c)[5]. In 1981, an improved patch clamp technique with a very high resistance was reported[6]. This technique, which was called gigaseal, offered an improved signal-to-noise ratio and allowed very small currents to be recorded. After its introduction, patch clamp technology became widely adopted, and today, automatic patch clamps are available that can record numerous single ion channels simultaneously. The patch clamp can thus be considered as the first generation of neural interfaces.

Multi-channel neural interface devices

The second generation neural interface enabled multi-channel in vivo neural signal acquisition and stimulation. These devices alleviated the work of sample preparation in the patch-clamp technique and allowed direct wired communication to living subjects. The neural signals are interfaced through different neural electrodes according to the different types of neural signals of interest. A cable is used to connect the electrodes and the signal processing workstations. Both signal acquisition from the living subject and neural stimulation to the subject are enabled.

Specification of neural signals acquired using different types of electrodes. Conventional electrophysiology focused on intracellular recording of the peripheral nervous system and was only applicable to a single neuron with the electrodes placed inside and outside the membrane. Intracellular recording only measures voltages across

[1]Department of Electronic Engineering, Tsinghua University, Beijing, China. [2]Department of Electrical and Systems Engineering (ESE), University of Pennsylvania, Philadelphia, PA, USA. ✉e-mail: zhangmilin@tsinghua.edu.cn

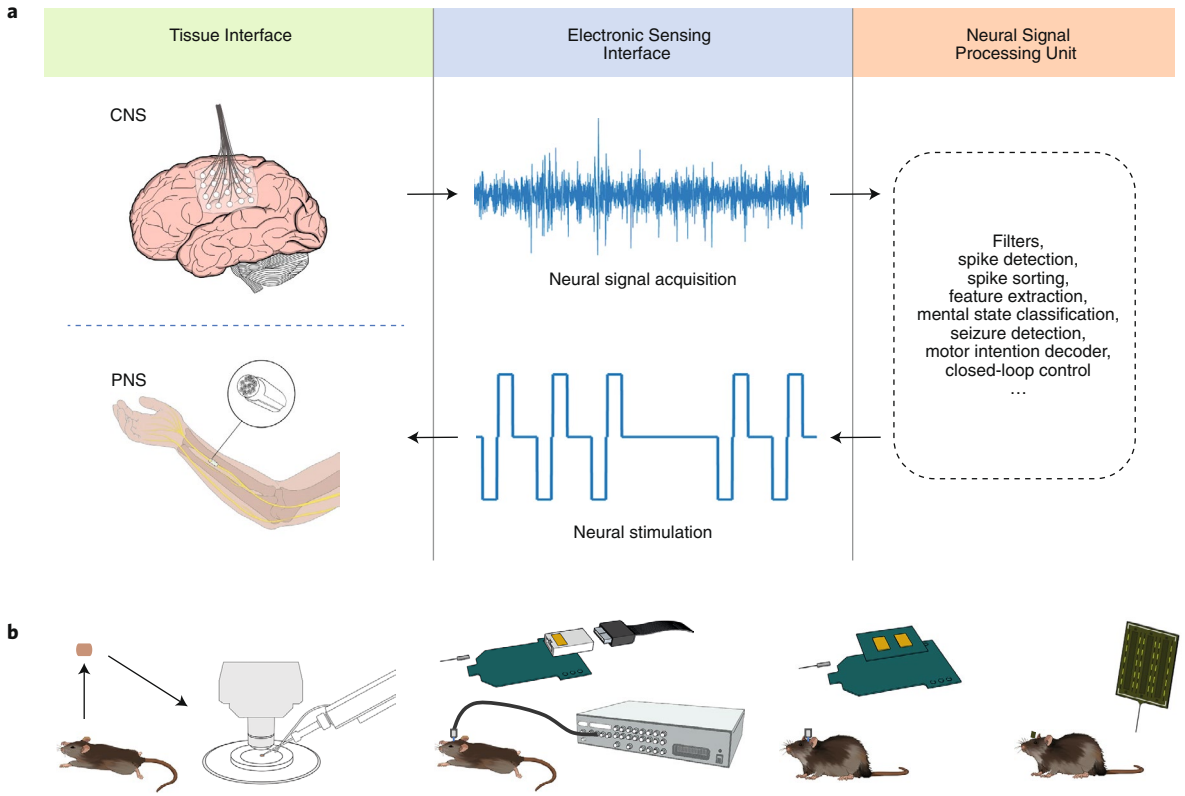

Fig. 1 | The development of neural interfaces. a, In order to directly communicate between the digital world and the nervous system, three key modules are required: a tissue interface, which translates biological neural activities from the central nervous system (CNS; with, for example, electrocorticography electrodes) or the peripheral nervous system (PNS; with, for example, cuff electrodes) into electrical signals (such as voltage, current or impedance); a sensing interface, including a neural signal acquisition module for signal amplification and digitization, and/or a neural stimulation module to elicit the activities of a neuron; and a neural signal processing unit. **b**, Based on technical milestones in the development of the sensing interface, neural interfaces can be roughly divided into four generations. The first generation (left) enabled in vitro neural signal acquisition from samples taken from subjects. The second generation (middle-left) enabled in vivo neural signal acquisition and stimulation, but a cable was required to get access to the workstation for signal processing and control. Standard connectors were applied to link the tissue interface and the sensing interface. The third generation (middle-right) offered wireless and lightweight sensing interfaces, but the tissue interface and the sensing device were still separated. The fourth generation (right) integrated the tissue interface and the sensing interface on the same substrate, creating a monolithic neural interface.

the cell membrane, but is able to capture sub-threshold deviations from resting potentials. For extracellular recordings, the electrodes are typically placed in the extracellular fluid and record signal summations generated by nearby neurons. The extracellular neural signal features reduced amplitudes as compared to the intracellular recording, but it records neural activities over a larger area.

Based on the location of the electrodes, extracellular recordings can be classified into either non-invasive or invasive methods. Non-invasive methods record from the surface of the scalp and are called electroencephalography (EEG). Invasive methods use electrodes placed inside the body and includes electrocorticography (ECoG), where electrodes are placed under the skull on top of the cerebral cortex, and local field potential (LFP), where electrodes are usually placed inside brain tissue[7] (though LFP can also be acquired using ECoG electrodes[8]). Using miniaturized electrodes made with flexible substrates, micro-electrocorticography (μECoG) arrays have also been developed, which offers higher spatial and temporal resolution than traditional ECoG. The invasive approach enables a more direct interaction with neurons, resulting in higher signal-to-noise ratios and higher-frequency signal bands, as well as improving stimulation effectiveness and accuracy (Fig. 3a).

Different types of electrodes are used depending on the signal acquisition method. For non-invasive extracellular recordings, the acquisition of EEG signals is challenging due to the weak amplitude of the signal and the difficulties in achieving a good contact between the electrode and the scalp, since poor contact can easily introduce noise. Traditional EEG wet electrodes are made of metals (such as gold, platinum, silver/silver chloride, and tin), and gels are mounted in the elastic caps to improve signal quality. Dry electrodes without gels are more convenient and feature a comparable performance to the wet electrodes[9]. However, dry electrodes suffer from higher electrode–tissue impedance and a low robustness to moving artefacts, and wet electrodes are still regarded as the gold standard for lab environments. To address this problem, active electrodes with integrated preamplifiers placed close to the electrodes have been developed[10]. Recently, EEG electrodes using new material and design structures have been reported, including polymer foam electrodes, flexible metal-coated polymer bristles, injection moulded dry electrodes and soft conductive textiles electrodes[9]. Standards for the position of electrode placement have also been developed, from an initial 19 electrode positions[11], to a more recent 300 electrode positions[12].

Electrodes used for invasive signal acquisition can be divided into two categories: penetrating and non-penetrating electrodes. Invasive non-penetrating cortical electrodes (Fig. 3b) include epidural ECoG electrodes, which are placed on the dura mater, and subdural ECoG electrodes, which are placed on the arachnoid. Conventional ECoG electrodes usually feature a pitch of around 1

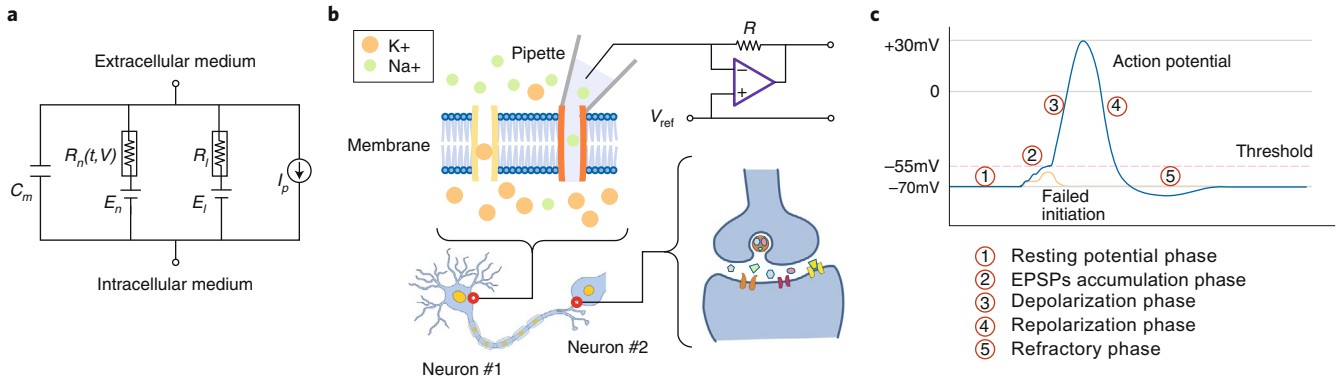

Fig. 2 | The electrophysiology behind the patch clamp technology. a, Hodgkin–Huxley model describing the membrane potentials using an RC circuits model[4]. The model captures the mathematical description of the action potentials mechanism. R_l and R_n represent the linear and non-linear leaky ion channels, respectively. E_l and E_n represent the linear and non-linear electrochemical driving voltage, respectively. I_P represents the ion pumps. **b**, Schematic illustrating patch clamp recording, including circuits of the technique, of an ion channel (top) and the mechanism of neural propagation (bottom). In a patch clamp, a hollow glass tube with a recording electrode (a glass pipette electrode) makes contact with the cell membrane. With a gentle suction, a patch of the membrane can be isolated electrically from the external solution, so that a single ion channel can be individually recorded. The neural signal propagates along the membrane of the neuron until it reaches the end of the axon. Here, neurotransmitters are released from synaptic vesicles by the presynaptic neuron. Receptors on the dendrite of the postsynaptic neuron receive the neurotransmitters, and generate excitatory postsynaptic potentials (EPSPs). **c**, Amplitude waveform of an action potential. When a neuron is in the idle state (resting state), the interior of the membrane has a resting potential of around −70 mV compared to the exterior of the membrane. This voltage is maintained by the permeability dominated by the Na+ and K+ ion channels[135]. The postsynaptic neuron will produce an action potential spike if sufficient EPSPs in the dendritic arbor cause the membrane potential to exceed a threshold. When the neuron becomes active, the voltage between the interior and exterior membrane changes quickly to a positive value as a result of inflow of Na+ ions during the depolarization phase. The voltage drops after reaching the peak of around 30 mV as a result of closing of the Na+ channels and a simultaneous outflow of K+ ions during the repolarization phase. The voltage continues to drop and overshoots initial resting potential and finally after the refractory phase it returns to the idle state at -70 mV. This sharp change of neural membrane voltage is named the action potential. The invoked action potential propagates along the axon and provokes action potential of the neighbouring neurons successively. This mechanism is the basis of neuronal communication.

cm (ref. [13]). Flexible μECoG electrodes push the spatial resolution down to the millimetre or even sub-millimetre range[14]. Flexible substrates also reduce the effective distance between source and electrodes through tight, conformal geometries[15]. Recent transistor multiplexed ECoG arrays have further reduced the area for routing wires, as well as increased the electrode density and channel count[16,17].

For penetrating electrodes, microwires made of stainless steel, tungsten or platinum/iridium, and insulated with biocompatible materials, are widely used[18,19]. Bundled arrays of 4 microwires known as tetrode yield better mechanical stability and improved performance of spike sorting[20]. Recently a DARPA funded program has been announced to develop a neural input–output bus (NIOB) to interface with up to one million neurons with tightly bundled microwires[21]. This technique faces challenges in signal attenuation, between channel crosstalk and interference. An alternative solution that enables multiple site recording is to use silicon-based microelectrodes fabricated in the shape of needles[22–24] (Fig. 3c). However, the rigid probes may cause tissue damage and inflammation, and as a result degrade the recording signal. Flexible penetrating electrodes made of polymers are more friendly for chronic implants[25] (Fig. 3d). The flexibility, however, makes the insertion difficult, since the electrodes bend and deflect easily. A robotic approach for effective polymer electrode insertion has also been introduced[26]. Another approach to reduce the tissue response is to minimize the footprint of the electrodes, as achieved with carbon fibre electrodes with cross-sections of several micrometres[27]. High density arrays of carbon fibres have also been developed for reliable insertion methods[28,29] (Fig. 3e).

Initially, microwires were used in work on the peripheral nervous system, but they are were not widely used now due to the damage they can cause to the subject's nerves. An alternative solution is to use thin flexible intra-fascicular electrodes, such as the longitudinally intra-fascicular electrodes (LIFE)[30], and the transverse intra-fascicular multi-channel electrodes (TIME)[31]. Experiments show promising future of intra-fascicular electrodes to serve as prosthetic solutions[32]. Sieve electrodes (also known as regenerative electrodes)[33] with arrays of holes enable the transected nerves to regenerate axons. The axons are held by the guiding tube and grow through the holes and connect with the distal end. The axons contact the conductive region surrounding the hole, enabling neural signal recording and stimulation. The prominent non-penetrating peripheral electrodes are the cuff electrodes (Fig. 3f), which are widely used in the study of neural pathways. The silicone wraps around the nerve with metal electrodes on the interior surface that contact the nerve inside[34].

Novel electrodes, including those based on organic materials, meshes, and multi-functional flexible polymer fibres, are also being developed with higher spatial integration, improved long-term stability and better biocompatibility than conventional electrodes[35].

Types of neural stimulation. Electrical stimulation modulates the nervous system by applying charges to the neurons. The electrode–tissue interface can be modelled as a double layer capacitor with a resistor in parallel; a voltage source is in series with the resistor to model the electrochemical potential[36,37] (Fig. 4a). There are three different stimulation patterns: unipolar (monopolar) stimulation (Fig. 4c), bipolar stimulation (Fig. 4d) and multipolar stimulation (Fig. 4e). Although the theory underlying neural stimulation is not fully understood, it has been widely used to study the propagation mechanisms in neuron networks by recording the response to well controlled stimulation patterns (Fig. 4b). It has also been used in clinical practice to reduce the symptoms of neurological disorders, such as seizures, Parkinson's disease and pains.

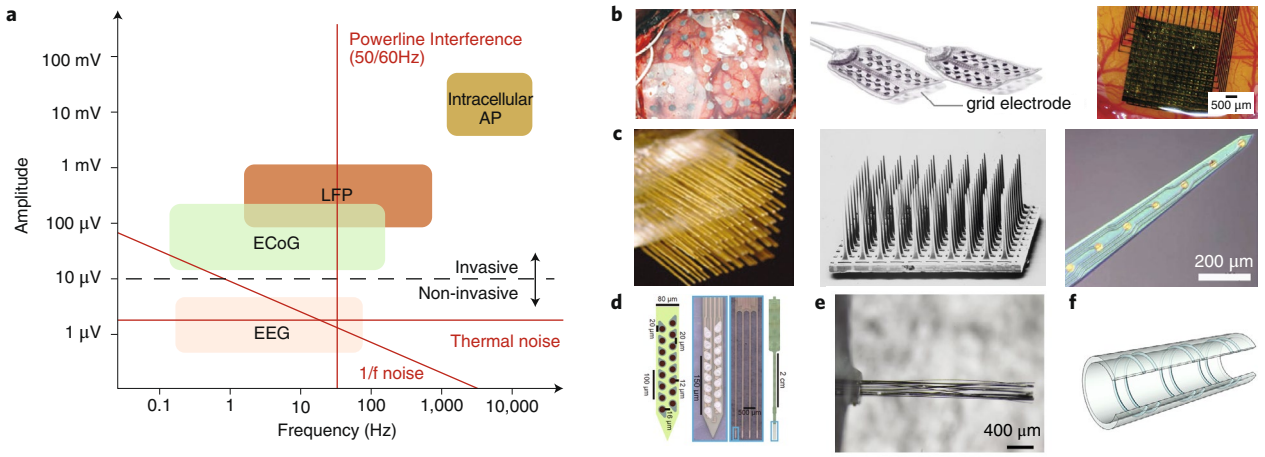

Fig. 3 | Typical neural signal characteristics and neural electrodes. a, The amplitude and frequency range of neural signals. The red lines represent the common internal 1/*f* and thermal noise from the electronic circuits itself and external powerline interference that may degrade the quality of neural signal recording. The extracellular AP amplitudes are usually lower than that of intracellular AP, and depend on the method for recording and the proximity of the neuron to the electrode. Thermal noise has nearly constant power spectral density (PSD) throughout the whole frequency spectrum, and the magnitude of the PSD is approximately several μV. The 1/*f* noise has the PSD reversely proportional to the frequency. The 50/60 Hz powerline interference is another major noise source that could easily be coupled into the neural recording front-ends. **b**, Typical invasive non-penetrating electrodes for ECoG recording. Conventional ECoG electrodes usually feature a pitch of around 1 cm (left). Flexible μECoG electrodes have pitches of several millimeters (middle). Recent trends in transistor-multiplexed ECoG arrays reduce the area for routing wires, as well as increase the density and channel count (right). **c**, Invasive microelectrodes fabricated in the shape of needles for penetration into the brain tissue, for example, microwire (left), Utah array (middle), and Michigan array (right). **d**, Flexible penetrating high-density polymer electrodes. **e**, High-density carbon fibre electrode array. **f**, Cuff electrodes, the non-penetrating peripheral electrodes, can wrap around the nerve with metal electrodes on the interior surface. Figure adapted with permission from: **b** (left), ref. [13], IOP; **b** (middle), ref. [94], Taylor & Francis under CC BY-NC-ND 4.0; **b** (right), ref. [17], APS; **c** (left), ref. [19], © PNAS; **c** (middle), ref. [23], Elsevier; **c** (right), ref. [24], Wiley; **d**, ref. [25], Elsevier; **e**, ref. [29], IOP.

Based on the application, stimulation can be applied to different sites of the nervous system. This can be, for example, transcranial electrical stimulation (tES) for pain suppression, which uses electrodes placed on the scalp over the area of interest of the brains[38]; spinal cord stimulation (SCS) for pain suppression and restoration of movement in paralyzed patients, which directly stimulates the spinal cord[39]; deep brain stimulation (DBS) for pain suppression, seizure suppression, and treatment of Parkinson's disease and mental depression, which places penetrating electrodes deep inside the brain tissue[40]; vagus nerve stimulation (VNS) for treatment of tinnitus, drug-resistant epilepsy and depressions[41]; transcranial magnetic stimulation (TMS) for depression treatment, which generates magnetic fields from outside the skull and cause electric currents at the targeted brain area[42]; or stimulations applied to the auditory nerve or optic nerve, which are used in cochlear and retinal prostheses to restore the hearing and vision, respectively.

Various workstations have been developed that act as the electronic multichannel interface to different types of electrodes. The electrodes (discussed above) are connected through wires to the workstations for signal digitization, signal processing and stimulation control. The use of workstations has helped boost advances in neuroscience research, and is one of the most common devices used in neuroscience labs. However, the bulky size prevents its use in various studies, including those on freely moving subjects and research that requires long-term, continuous recording. Systems with smaller size but comparable functionality are needed.

Implantable/wearable neural interface devices

Compact, cable-free devices, which use custom application-specific integrated circuits (ASICs) and printed circuit board (PCB) level integration, have now been developed and we term these implantable/wearable devices the third generation of neural interfaces. Wireless communication of control signals and data are implemented using either commercial solutions or customized designs, and signal processing is possibly achieved on a separate computer, a general-purpose microcontroller, or an ASIC.

There are a number of design considerations in the development of compact, implantable/wearable neural interfaces. These include safety (implanted electrodes and the stimulation and recording electronics must cause minimal damage to the tissue) and reliability (for example, signal recording quality consistency, data link/storage stability, signal processing accuracy, and physical electrode connection reliability). There is also flexibility (recording and stimulation with programmable amplification gain, bandwidth, channel selection, sampling rate, and/or stimulation parameters) and portability (the size miniaturization of the entire system is important, particularly for research on freely moving subjects, and this requires electronic devices with small areas and compact integration techniques). And low power consumption (with the limitation of the system size, a lower power consumption will bring longer battery life for long-term experiments, as well minimizing tissue damage due to dissipated heat) and fast artefact cancellation (simultaneous neural stimulation would cause saturation in neural acquisition front-ends).

The use of custom designed systems offers the potential to significantly reduce size and power consumption. It optionally consists of a neural acquisition module, a neural stimulation module, a feature extraction/signal processing module, and a closed-loop control module. Table 1 summarizes state-of-the-art closed-loop neural interface systems-on-chip. The neural signal acquisition front-ends requires low input-referred noise[43,44], sufficient dynamic range[45,46], high input impedance[47], high linearity[47,48], high common-mode rejection ratio (CMRR)[49], and high power-supply rejection ratio (PSRR)[50].

Noise efficiency factor (NEF) is widely accepted as a figure-of-merit, which is the noise produced by the neural acquisition front-end amplifier compared to one single bipolar transistor with the same bias current, and represents the trade-offs of these requirements

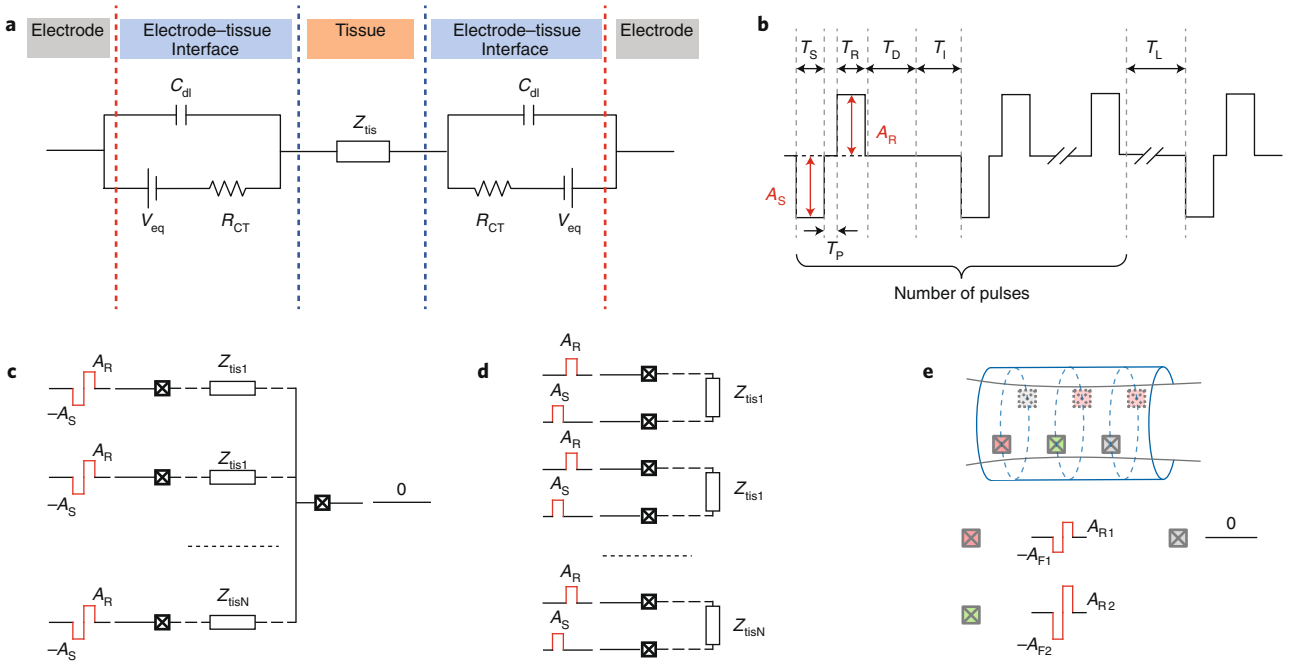

Fig. 4 | Electrode–tissue interface model and stimulation waveform patterns. a, The circuits model of the electrode–tissue interface. Z_{tis} represents the impedance of the tissue. The capacitor C_{dl} represents the charges stored at the interface, and the resistor R_{CT} mimics the electrochemical processes, such as the oxidation reactions. To model the electrochemical potential that acts as the driving force for chemical processes, a voltage source V_{eq} is added in series with the resistor. **b**, A typical biphasic stimulation waveform with adjustable amplitude, pulse width and stimulation intervals. A_S is the stimulation voltage/current amplitude. A_R is the reversal voltage/current amplitude. T_S is the stimulation phase time. T_R is the reversal phase time. T_D is the discharging phase time. T_P is the phase interval. T_I is the pulse interval. T_L is the pulse group interval. Typical amplitudes of A_S and A_F vary from 100 μA to 1 mA for current mode stimulation, and from 2 V to 10 V for voltage mode stimulation, respectively. **c**, The unipolar (monopolar) stimulation, which is widely used in high-density electrode arrays. It delivers a stimulus with respect to a common reference electrode. **d**, The bipolar stimulation, which allows for a better directed stimulation than the monopolar stimulation, at the cost of a more complicated channel selection control logic. The bipolar stimulation can be implemented using either a single power supply or multiple power supplies. The single power supply system is favored since it doubles the compliance voltage range. **e**, The multipolar stimulation employs multiple electrode sites with different biphasic patterns to stimulate the target tissue. Selective sites are configured with different stimulation patterns. For example, the cuff electrode with multiple sites could be configured as illustrated.

in circuit design[51]. Other figures-of-merit, such as the power efficiency factor (PEF) and the system efficiency factor (SEF), are also used to evaluate the performance of the acquisition front-ends. Traditional neural acquisition front-ends employ the AC-coupled amplifier to block the large input DC offset and boost the input impedance[43,44]. The DC-coupled amplifier reduces the large area of the blocking capacitors but may degrade CMRR[52,53]. To achieve sufficient dynamic range, which is essential in bidirectional neural interfaces, recent trends directly convert the analogue signal without the amplifiers, either using the ΔΣ modulators[45,46,54–56] or the time-based recording front-ends[48,57,58].

There are three predominant categories of stimulators. Voltage mode stimulators features higher energy efficiency and simpler circuits[59]. However, due to the variability of the impedance of the electrode tissue interface, the amount of charge transferred to the tissue is hard to control and to balance. Current mode stimulators improve the control of charges, but sacrifice energy efficiency[60,61]. Switched-capacitor mode stimulators achieve both high efficiency and accurate charge control, but consume large area of on-chip capacitors[62]. Charge accumulation at the electrode tissue interface should be avoided for biosafety concerns. Biphasic waveform stimulation enables better control of charge-balance. However, even with careful design of the symmetry of anodic and cathodic stimulation phases, dynamic charge monitoring and balancing methods[60,63] are preferable in state-of-the-art stimulation designs[60–62].

On-chip neural signal processing and feature extraction. Various neural signal processing methodologies have been developed to understand neural activity and subject behaviour. Here we highlight general purpose neural signal processing methods that have been implemented on-chip, as well as the control of a closed-loop neural interface. A key aspect of a closed-loop neural interface is the ability to process signals and extract discriminative features. Traditional MCUs or DSPs can be customized for biomedical applications[64–66], but the power efficiency is low, compared to custom designed neural signal processing units.

On-chip signal processing systems optimized for neural interfaces can be divided into three categories: neural signal feature extraction, data compression prior to data transmission and closed-loop control-orientated modules.

Neural signal feature extraction, including neural energy in specified frequency bands[67,68], AP spikes[69], frequency-time wavelet domain features[70], entropy[71], and phase synchrony[55,56], have been widely applied. Some work directly extracts the high level features, such as the detection of neurological disorder onset[55,68,72], sleep staging[72–74] and decoding of movement intentions[75]. Applying neural signal feature extraction online before data transmission can advance the functionality of the system from data acquisition into information acquisition. Neural signals with a certain cognitive state can be situated in a very narrow frequency band, especially in the low frequency range. The commonly used neural signal frequency sub-bands include the delta band in 0.5–3 Hz, theta band in

Table 1 | Comparison of state-of-the-art neural interface systems-on-chip

	Acquisition						Stimulation					System level		
	Ch #	Band width	V_{rms} (μV)	Gain (dB)	NEF	Power (μW ch^{-1})	Ch #	Stim. mode	Max. current (mA)	On-chip signal processing	Wireless datarate (kbps)	Power (mW)	Area	Technology
Stanslaski 2018[92]	4	LFP/ECoG	Unknown	48	Unknown	5	8	Current	25.5	FFT, SVM	195	2.5	13.9 cm^3 (die stacking)	0.8 μm, 0.25 μm
Azin 2011[69]	8	0.5–50k	3.12	51.9–65.6	2.68	26.9	8	Monophasic/ biphasic current	0.0945	DSP; time amplitude window	Unknown	0.375	10.9 mm^2	0.35 μm
Rhew 2014[67]	4	0.64–6k	6.3	54	3.76	61.25	8	Biphasic current	4.18	Filter; energy detection; PI controller	800	0.468	4 mm^2	180 nm
Cheng 2018[71]	16	0.59–117	2.09	50, 60, 70	3.78	Unknown	16	Biphasic current	3	Approximate entropy; power spectral density; ridge regression classifier	106	54	25 mm^2	180 nm
Kassiri 2017[55]	64	0.01–500	1.13	–	2.86	0.63	64	Arbitrary current	1.35	Filter; phase synchrony	46000	5.44	5.98 mm^2	130 nm
Altaf 2015[68]	16	0.5–100	0.9	52	3.29	1.62	1	Voltage	–	Band energy; D2A LSVM	–	Unknown	25 mm^2	180 nm
O'Leary 2018[56]	32	0.1–1k	1.6	–	2.86	1.26	32	Arbitrary current	3	Phase-locking value; cross-frequency coupling; band energy; EDM SVM	–	0.6744	7.59 mm^2	130 nm
Pazhouhandeh 2019[72]	64	0.1–5k	2.1	–	2.98	0.79	64	Arbitrary current	Unknown	Band energy; EDM SVM	Unknown	Unknown	11 mm^2	130 nm

3–8 Hz, alpha band in 8–12 Hz, beta band in 12–38 Hz and gamma band in 38–100 Hz. This presents a serious design challenge in the energy extraction circuit. Neural energy detectors have been created in both analogue[76,77] and digital domains[56,68]. The digital implementation could easily tune the energy band by changing the filter coefficient registers. In the analogue implementation, band tuning is more difficult, but with relatively lower power consumption.

On-chip single AP spike detection can be achieved based on either time-domain amplitude features or energy-domain features. Dual-threshold time-domain methods with fixed or adaptive thresholds have been widely used for AP spike detection for its simplicity. Energy-domain methods (that is, non-linear energy operator (NEO)[78]) features higher robustness. Some AP detection ASICs based on novel algorithms, such as the exponential component-polynomial component (EC-PC) engines[79], have been reported. Several key AP features can be extracted during single AP detection, including maximum/minimum spike amplitude, spike width, and the derivatives of spikes[78]. Spike sorting is a widely applied online processing method. Methods such as principal component analysis (PCA)[80] and K-means clustering[81,82] aim to achieve a good balance between algorithm complexity, power consumption, and storage requirements.

For online data compression, compressed sensing is widely used in implantable/wearable neural interfaces[83–85] due to the simplicity of the encoding process. Data selection is another way to reduce the data transfer throughput. With on-chip signal processing, data could be transmitted only when interested neural activity (AP spikes, for example) are detected, or only extracted neural features are transmitted instead of the raw data[70,86,87].

Closed-loop control-oriented modules play an important role in real world applications. Stimulations can be triggered by AP spikes[69], detected specific features[68,71] or controlled by PID[67,88]. The implementation of closed-loop control requires integration of both the analogue recording front-end and the analogue stimulating back end in the same system or even on a single die. The strong stimulation signal easily saturates the amplifier in the recording front-end, which is denoted as the stimulation artefact. Reducing the effects of the stimulation artefact becomes a key challenge in closed-loop system design. Various solutions have been investigated. These include blanking technique, which cuts off recording for a short period after the stimulator was triggered[89]; it is simple but leads to undesired missing information. Alternatively, the strength of the artefact can be reduced in the analogue domain[45] with saturation prevention or rapid recovery. The effect can also be reduced by performing digital signal processing[48,90] with signal interpolation or artefact subtraction. However, none of these methods have provided an adequate solution to reduce the impact of the artefacts, and co-design of these techniques could be used in the future research[91].

Applications of implantable/wearable neural interface. Neural stimulation has been proved to be effective in the treatment of many neurological disorders. Closed-loop neuromodulation devices are available for daily use, such as Medtronic Summit RC+S system[92], Neuropace RNS system[93] and CorTec Brain Interchange system[94].

The development of wearable neural interface devices benefits from the development of the integrated circuits. Various non-invasive EEG health monitors are available on the market, such as the IMEC EEG headset[95]. Another trend is the integration of multi-modal recording front-ends on the same chip[96]. Hybrid neural interfaces[97], which combine different neural signals to reveal additional information to improve the performance of the neural interfaces, could also benefit from this multi-modal neural signal recording integration. Various compact neural interfaces used in freely moving animal subjects for neuroscience research, aiming to better understand the causality between the behaviour and the activity of the nervous system have also been reported[98–101].

Motor intention could be decoded from neural signals recorded either invasively[102,103] or non-invasively[104]. Neural interfaces can also allow disabled people to control wheelchair movements[105] and to communicate with others[106]. Although the neural interface prosthetic arms and hands are currently limited to lab use, the miniaturization of the electronic devices will help put them in clinical practice in the near future. Neural stimulation has been used in cochlear implants for a long time, and retinal stimulation prosthesis could also be used to help improve eyesight[107].

Many clinical trials have illustrated the efficacy of neural interfaces for neurological disorder rehabilitation such stroke recovery[108]. Experiments on non-human primates[109] and humans[110] show that it is promising to bypass the wound in the neural pathway and rebuild the neural signal communication for paralyzed people with spinal cord injuries. With the help of electronic skin[111], tactile sensing can be restored by stimulating the peripheral nervous system[32] or the central nervous system[112].

To translate implantable/wearable neural interfaces from the lab to consumer products, a number of challenges need to be addressed. There is, to start, a lack of a deep understanding of how the nervous system works from a medical point of view. Power efficiency from a circuits and systems point of view needs to be improved. There is an uncertainty in the biosafety of long-term implantations from a material and device point of view. The degraded quality of recorded signal in the presence of tissue encapsulation remains an issue, which can also lead to increased power consumption because signals are attenuated by scarring tissue.

Integrated neural interfaces

In order to achieve high density neural recording and stimulating sites, and reduce the damage caused by the implanted device, integrated neural interfaces are being developed, which combine the circuits and the neural probes onto the same base; these devices we term the fourth generation of neural interfaces. In comparison, third generation neural interfaces involve the PCB integration of the probes and IC chips. The size of the device is dominated by the PCB, thus limiting further miniaturization.

For fourth generation interfaces, state-of-the-art devices can, for example, feature 966 recording sites for active electrodes[113] and 1,600 recording sites for passive electrodes[114]. From a circuits point of view, the main drawback of such work is the relatively large base area required to implement a multiplexer or/and the buffer and analogue-to-digital-convertor (ADC) circuits, causing large skull damage compared to the thin and long recording needle. To address this, devices that remove the base part by implementing on-site ADC and using global analogue lines have been developed, enabling fully immersible electrodes for recording with minimal tissue damage[115]. Though the resulting integrated neural interfaces are still rigid and not very suitable for chronic implants, the approach could possibly take the advantages of substrate transfer technology[116], and could, in the future, be used to create fully integrated flexible monolithic neural interfaces.

Ultra-small implantable free-floating neural interface devices with wireless powering and data transmission are also now emerging. Conventional invasive neural probes can only record or stimulate a small area of the brain, but these millimetre-scale devices could be freely distributed, interfacing a larger area of the nervous system, which may reveal higher-level mechanisms of brain functionalities. Conventional electrodes integration methods, such as bondwire or flip-chip technology[54,117], are being reformed by on-chip electrodes[118] or microwire insertion through through-silicon-via (TSV)[119]. External coil[54] could also be replaced by on-chip coil[118,120]. Die dicing and post processing methods have also been used to form the electrodes on the side face of the chip, creating an ultra-small 0.009 mm^3 neural stimulating system[120]. Since a magnetic field is severely attenuated by tissue, relay coil are often placed on the surface of the cortex[119,121,122]. This problem can be solved by using ultrasound for powering and data transmission instead of traditional magnetic fields[123–125]. While most state-of-the-art devices feature one directional single channel interface, systems capable of 8-channel simultaneous recording have been developed[126]. The issue of management of multiple free-floating neural interfaces, such as data isolation and analysis, remains though to be addressed[127].

Advances in complementary metal–oxide–semiconductor (CMOS) technology are pushing neural interface circuit and system design towards monolithic, fully-integrated designs, featuring a smaller size, a lower power consumption, a higher acquisition density, and real-time online feature extraction/machine learning, compared to traditional high cost neural interfaces with limited processing abilities. These interfaces, however, place greater demands on circuits and systems designers.

Benefiting from the high integration, the density of contacts are being greatly improved with fourth generation neural interfaces. The emergence of these fourth generation neural interfaces also enables the possibility of implanting more than one device into a living body. Wireless communications between the multiple neural interface devices could also be used to form an artificial network parallel to the brain's neural network. But new questions arise with such developments, including how to deliver massive data communication (up to several Gbps) between different devices, as well as between the devices and living tissues; how to efficiently power up the implanted devices; and how to protect the security of the data. In order to reduce the power consumption, on-chip signal processing could be integrated to reduce the workload of the transceiver. Only data with certain characteristics, or only extracted neural markers, would be transmitted. On chip closed-loop control modules could even manage the neural interfaces itself without continuous communication with the external devices.

This will deliver a higher throughput in translating neural activity into machine language. The increasing throughput of neural signal acquisition, as well as the increasing precision in neural stimulation control, could enable the establishment of an effective artificial neural sensing capability. This brings an ethical dilemma to the design: how much intelligence or decision-making authority should be granted to the device, and what is a best trade-off between efficiency and safety.

We have focused here on electronic neural interfaces, but there are other ways to impact neural activity. Ultrasound can be steered non-invasively and stimulate the nervous system at a millimetre scale[128], though no electronically integrated devices have been reported to date. Light can be used instead of electronic charges for neural stimulation[122,129]. The control of single ion channels using optogenetics was first introduced in 2005[130,131]. Light activated proteins are expressed in targeted neurons and response to light with different wavelengths, enabling a selection of stimulation targets. This, however, requires complicated chemical and biological preprocessing of the cells, which is not always suitable for human subjects. Nevertheless, recent research highlights the possibility of implementing wireless optogenetics-based neural stimulation without waveguides[132]. A combination of needle-shaped electronic

neural interfaces and fibre-based optical neural interfaces could lead to a new generation of brain–machine interfaces[133,134].

Received: 20 June 2019; Accepted: 2 March 2020;
Published online: 13 April 2020

References

1. Galvani, L. *De Viribus Electricitatis In Motu Musculari Commentarius Bologna* (Academy of Sciences, 1791).
2. Marmont, G. Studies on the axon membrane. I. A new method. *J. Cell. Compar. Physiol.* **34**, 351–382 (1949).
3. Hodgkin, A. L. & Huxley, A. F. Currents carried by sodium and potassium ions through the membrane of the giant axon of loligo. *J. Physiol.* **116**, 449–472 (1952).
4. Hodgkin, A. L. & Huxley, A. F. A quantitative description of membrane current and its application to conduction and excitation in nerve. *J. Physiol.* **117**, 500–544 (1952).
5. Neher, E. & Sakmann, B. Single-channel currents recorded from membrane of denervated frog muscle fibres. *Nature* **260**, 799–802 (1976).
6. Hamill, O. P., Marty, A., Neher, E., Sakmann, B. & Sigworth, F. Improved patch-clamp techniques for high-resolution current recording from cells and cell-free membrane patches. *Pflüg. Arch.* **391**, 85–100 (1981).
7. Buzsáki, G., Anastassiou, C. A. & Koch, C. The origin of extracellular fields and currents—EEG, ECoG, LFP and spikes. *Nat. Rev Neurosci.* **13**, 407–420 (2012).
8. Konerding, W., Froriep, U., Kral, A. & Baumhoff, P. New thin-film surface electrode array enables brain mapping with high spatial acuity in rodents. *Sci. Rep.* **8**, 3825 (2018).
9. Lopez-Gordo, M., Sanchez-Morillo, D. & Valle, F. Dry EEG electrodes. *Sensors* **14**, 12847–12870 (2014).
10. Xu, J., Mitra, S., Van Hoof, C., Yazicioglu, R. F. & Makinwa, K. A. Active electrodes for wearable EEG acquisition: review and electronics design methodology. *IEEE Rev. Biomed. Eng.* **10**, 187–198 (2017).
11. Klem, G. H., Lüders, H. O., Jasper, H. & Elger, C. et al. The ten-twenty electrode system of the international federation. *Electroen. Clin. Neurophysiol.* **52**, 3–6 (1999).
12. Jurcak, V., Tsuzuki, D. & Dan, I. 10/20, 10/10, and 10/5 systems revisited: their validity as relative head-surface-based positioning systems. *Neuroimage* **34**, 1600–1611 (2007).
13. Leuthardt, E. C., Schalk, G., Wolpaw, J. R., Ojemann, J. G. & Moran, D. W. A brain–computer interface using electrocorticographic signals in humans. *J. Neural Eng.* **1**, 63–71 (2004).
14. Tolstosheeva, E. et al. A multi-channel, flex-rigid ECoG microelectrode array for visual cortical interfacing. *Sensors* **15**, 832–854 (2015).
15. Blau, A. et al. Flexible, all-polymer microelectrode arrays for the capture of cardiac and neuronal signals. *Biomaterials* **32**, 1778–1786 (2011).
16. Khodagholy, D. et al. In vivo recordings of brain activity using organic transistors. *Nat. Commun.* **4**, 1575–1575 (2013).
17. Escabí, M. A. et al. A high-density, high-channel count, multiplexed μECoG array for auditory-cortex recordings. *J. Neurophysiol.* **112**, 1566–1583 (2014).
18. Lehew, G. & Nicolelis, M. A. in *Methods for Neural Ensemble Recordings* 2nd edn (ed. Nicolelis, M. A.) Ch. 1 (Taylor & Francis, 2008).
19. Nicolelis, M. A. et al. Chronic, multisite, multielectrode recordings in macaque monkeys. *Proc. Natl Acad. Sci. USA* **100**, 11041–11046 (2003).
20. Buzsáki, G. Large-scale recording of neuronal ensembles. *Nat. Neurosci.* **7**, 446–451 (2004).
21. Obaid, A. M. et al. Massively parallel microwire arrays integrated with CMOS chips for neural recording. Preprint at https://www.biorxiv.org/content/10.1101/573295v1 (2019).
22. Wise, K. D., Anderson, D., Hetke, J., Kipke, D. & Najafi, K. Wireless implantable microsystems: high-density electronic interfaces to the nervous system. *Proc. IEEE* **92**, 76–97 (2004).
23. Rousche, P. J. & Normann, R. A. Chronic recording capability of the Utah intracortical electrode array in cat sensory cortex. *J. Neurosci. Meth.* **82**, 1–15 (1998).
24. Abidian, M. R. & Martin, D. C. Multifunctional nanobiomaterials for neural interfaces. *Adv. Func. Mater.* **19**, 573–585 (2009).
25. Chung, J. E. et al. High-density, long-lasting, and multi-region electrophysiological recordings using polymer electrode arrays. *Neuron* **101**, 21–31 (2019).
26. Hanson, T. L., Diaz-Botia, C. A., Kharazia, V., Maharbiz, M. M. & Sabes, P. N. The "sewing machine" for minimally invasive neural recording. Preprint at https://www.biorxiv.org/content/10.1101/578542v1 (2019).
27. Kozai, T. D. Y. et al. Ultrasmall implantable composite microelectrodes with bioactive surfaces for chronic neural interfaces. *Nat. Mater.* **11**, 1065–1073 (2012).
28. Patel, P. R. et al. Insertion of linear 8.4 μm diameter 16 channel carbon fiber electrode arrays for single unit recordings. *J. Neural Eng.* **12**, 046009 (2015).
29. Massey, T. L. et al. A high-density carbon fiber neural recording array technology. *J. Neural Eng.* **16**, 016024 (2019).
30. Lawrence, S. M., Dhillon, G. S. & Horch, K. W. Fabrication and characteristics of an implantable, polymer-based, intrafascicular electrode. *J.Nneurosci. Meth.* **131**, 9–26 (2003).
31. Boretius, T. et al. A transverse intrafascicular multichannel electrode (TIME) to interface with the peripheral nerve. *Biosens. Bioelectron.* **26**, 62–69 (2010).
32. Raspopovic, S. et al. Restoring natural sensory feedback in real-time bidirectional hand prostheses. *Sci. Transl. Med.* **6**, 222ra19–222ra19 (2014).
33. Akin, T., Najafi, K., Smoke, R. H. & Bradley, R. M. A micromachined silicon sieve electrode for nerve regeneration applications. *IEEE Trans. Biomed. Eng.* **41**, 305–313 (1994).
34. Nerve Cuff Electrodes. *MicroProbes for Life Science* (2020); https://microprobes.com/products/peripheral-electrodes/nerve-cuff
35. Hong, G. & Lieber, C. M. Novel electrode technologies for neural recordings. *Nat. Rev. Neurosci.* **20**, 330–345 (2019).
36. Merrill, D. R., Bikson, M. & Jefferys, J. G. Electrical stimulation of excitable tissue: design of efficacious and safe protocols. *J. Neurosci. Meth.* **141**, 171–198 (2005).
37. Van Dongen, M. & Serdijn, W. *Design of Efficient and Safe Neural Stimulators* (Springer, 2016).
38. Paulus, W. Transcranial electrical stimulation (tES–tDCS; tRNS, tACS) methods. *Neuropsychol. Rehabil.* **21**, 602–617 (2011).
39. Cameron, T. Safety and efficacy of spinal cord stimulation for the treatment of chronic pain: a 20-year literature review. *J. Neurosurg. Spine* **100**, 254–267 (2004).
40. Kringelbach, M. L., Jenkinson, N., Owen, S. L. & Aziz, T. Z. Translational principles of deep brain stimulation. *Nat. Rev. Neurosci.* **8**, 623–635 (2007).
41. Groves, D. A. & Brown, V. J. Vagal nerve stimulation: a review of its applications and potential mechanisms that mediate its clinical effects. *Neurosci. Biobehav. Rev.* **29**, 493–500 (2005).
42. Hallett, M. Transcranial magnetic stimulation: a primer. *Neuron* **55**, 187–199 (2007).
43. Luo, D., Zhang, M. & Wang, Z. A low-noise chopper amplifier designed for multi-channel neural signal acquisition. *IEEE J. Solid-State Circ.* **54**, 2255–2265 (2019).
44. Yaul, F. M. & Chandrakasan, A. P. A sub-μW 36nV/$\sqrt{\text{Hz}}$ chopper amplifier for sensors using a noise-efficient inverter-based 0.2V-supply input stage. In *IEEE Int. Solid-State Circuits Conference (ISSCC)* 94–95 (IEEE, 2016).
45. Johnson, B. C. et al. An implantable 700μW 64-channel neuromodulation IC for simultaneous recording and stimulation with rapid artifact recovery. In *2017 Symposium on VLSI Circuits* C48–C49 (IEEE, 2017).
46. Kim, C. et al. A 92dB dynamic range sub-μV_{rms}-noise 0.8μW/ch neural-recording ADC array with predictive digital autoranging. In *2018 IEEE Int. Solid-State Circuits Conference (ISSCC)* 470–472 (IEEE, 2018).
47. Chandrakumar, H. & Markovic, D. A 15.2-ENOB continuous-time ΔΣ ADC for a 7.3 μW 200 mV_{pp}-linear-input-range neural recording front-end. In *2018 IEEE Int. Solid-State Circuits Conference (ISSCC)* 232–234 (IEEE, 2018).
48. Rozgić, D. et al. A 0.338cm^3, artifact-free, 64-contact neuromodulation platform for simultaneous stimulation and sensing. *IEEE Trans. Biomed. Circ. Syst.* **13**, 38–55 (2018).
49. Ha, U. et al. An EEG-NIRS multimodal SoC for accurate anesthesia depth monitoring. *IEEE J. Solid-State Circ.* **53**, 1830–1843 (2018).
50. Lee, S. et al. A 110dB-CMRR 100dB-PSRR multi-channel neural-recording amplifier system using differentially regulated rejection ratio enhancement in 0.18 μm CMOS. In *2018 IEEE Int. Solid-State Circuits Conference (ISSCC)* 472–474 (IEEE, 2018).
51. Harrison, R. R. & Charles, C. A low-power low-noise CMOS amplifier for neural recording applications. *IEEE J. Solid-State Circ.* **38**, 958–965 (2003).
52. Zhao, Y., Shang, Z. & Lian, Y. A 2.55 NEF 76 dB CMRR DC-coupled fully differential difference amplifier based analog front end for wearable biomedical sensors. *IEEE Trans. Biomed. Circ. Syst.* **13**, 918–926 (2019).
53. Lee, B. & Ghovanloo, M. An adaptive averaging low noise front-end for central and peripheral nerve recording. *IEEE Transactions on Circuits and Systems II: Express Briefs* **65**, 839–843 (2017).
54. Muller, R. et al. A minimally invasive 64-channel wireless *μ*ecog implant. *IEEE J. Solid-State Circ.* **50**, 344–359 (2014).
55. Kassiri, H. et al. 27.3 All-wireless 64-channel 0.013mm^2/ch closed-loop neurostimulator with rail-to-rail DC offset removal. In *2017 IEEE Int. Solid-State Circuits Conference (ISSCC)* 452–453 (IEEE, 2017).
56. O'Leary, G. et al. A recursive-memory brain-state classifier with 32-channel track-and-zoom $\Delta^2\Sigma$ ADCs and charge-balanced programmable waveform neurostimulators. In *2018 IEEE Int. Solid-State Circuits Conference (ISSCC)* 296–298 (IEEE, 2018).
57. Jeon, H., Bang, J.-S., Jung, Y., Choi, I. & Je, M. A high DR, DC-coupled, time-based neural-recording IC with degeneration R-DAC for bidirectional neural interface. *IEEE J. Solid-State Circ.* **54**, 2658–2670 (2019).

58. Leene, L. B. & Constandinou, T. G. A 0.006mm² 1.2μW analog-to-time converter for asynchronous bio-sensors. *IEEE J. Solid-State Circ.* **53**, 2604–2613 (2018).
59. Haas, M. & Ortmanns, M. Efficient implementation and stability analysis of a HV-CMOS current/voltage mode stimulator. In *2018 IEEE Biomedical Circuits and Systems Conference (BioCAS)* https://doi.org/10.1109/BIOCAS.2018.8584804 (IEEE, 2018).
60. Butz, N., Taschwer, A., Manoli, Y. & Kuhl, M. 22.6 A 22V compliant 56μW active charge balancer enabling 100% charge compensation even in monophasic and 36% amplitude correction in biphasic neural stimulators. In *2016 IEEE Int. Solid-State Circuits Conference (ISSCC)* 390–391 (IEEE, 2016).
61. Greenwald, E. et al. A CMOS current steering neurostimulation array with integrated DAC calibration and charge balancing. *IEEE transactions on biomedical circuits and systems* **11**, 324–335 (2017).
62. Lee, H.-M., Kwon, K. Y., Li, W. & Ghovanloo, M. A power-efficient switched-capacitor stimulating system for electrical/optical deep brain stimulation. *IEEE J. Solid-State Circ.* **50**, 360–374 (2014).
63. Sooksood, K., Stieglitz, T. & Ortmanns, M. An active approach for charge balancing in functional electrical stimulation. *IEEE Transactions on Biomedical Circuits and Systems* **4**, 162–170 (2010).
64. Kwong, J. & Chandrakasan, A. P. An energy-efficient biomedical signal processing platform. *IEEE J. Solid-State Circ.* **46**, 1742–1753 (2011).
65. Cong, P. et al. A 32-channel modular bi-directional neural interface system with embedded DSP for closed-loop operation. In *European Solid State Circuits Conference (ESSCIRC)* 99–102 (IEEE, 2014).
66. Alzuhair, A. & Marković, D. A 216 nW/channel DSP engine for triggering theta phase-locked brain stimulation. In *2017 IEEE Biomedical Circuits and Systems Conference (BioCAS)* https://doi.org/10.1109/BIOCAS.2017.8325189 (IEEE, 2017).
67. Rhew, H.-G. et al. A fully self-contained logarithmic closed-loop deep brain stimulation SoC with wireless telemetry and wireless power management. *IEEE J. Solid-State Circ.* **49**, 2213–2227 (2014).
68. Altaf, M. A. B., Zhang, C. & Yoo, J. A 16-channel patient-specific seizure onset and termination detection SoC with impedance-adaptive transcranial electrical stimulator. *IEEE J. Solid-State Circ.* **50**, 2728–2740 (2015).
69. Azin, M., Guggenmos, D. J., Barbay, S., Nudo, R. J. & Mohseni, P. A battery-powered activity-dependent intracortical microstimulation IC for brain-machine-brain interface. *IEEE J. Solid-State Circ.* **46**, 731–745 (2011).
70. Iranmanesh, S. & Rodriguez-Villegas, E. A 950 nW analog-based data reduction chip for wearable EEG systems in epilepsy. *IEEE J. Solid-State Circ.* **52**, 2362–2373 (2017).
71. Cheng, C.-H. et al. A fully integrated 16-channel closed-loop neural-prosthetic CMOS SoC with wireless power and bidirectional data telemetry for real-time efficient human epileptic seizure control. *IEEE J. Solid-State Circ.* **53**, 3314–3326 (2018).
72. Pazhouhandeh, M. R. et al. 22.8 Adaptively clock-boosted auto-ranging responsive neurostimulator for emerging neuromodulation applications. In *2019 IEEE Int. Solid-State Circuits Conference (ISSCC)*, 374–376 (IEEE, 2019).
73. Imtiaz, S. A., Jiang, Z. & Rodriguez-Villegas, E. An ultralow power system on chip for automatic sleep staging. *IEEE J. Solid-State Circ.* **52**, 822–833 (2017).
74. Chang, S.-Y. et al. An ultra-low-power dual-mode automatic sleep staging processor using neural-network-based decision tree. *IEEE Trans. Circ. Syst. I* **66**, 3504–3516 (2019).
75. Chen, Y., Yao, E. & Basu, A. A 128-channel extreme learning machine-based neural decoder for brain machine interfaces. *IEEE Trans. Biomed. Circ. Syst.* **10**, 679–692 (2016).
76. Harrison, R. R. The design of integrated circuits to observe brain activity. *Proc. IEEE* **96**, 1203–1216 (2008).
77. Zhang, F., Mishra, A., Richardson, A. G. & Otis, B. A low-power ECoG/EEG processing IC with integrated multiband energy extractor. *IEEE Trans. Circ. Syst. I* **58**, 2069–2082 (2011).
78. Karkare, V., Gibson, S. & Markovic, D. A 130-μW, 64-channel neural spike-sorting DSP chip. *IEEE J. Solid-State Circ.* **46**, 1214–1222 (2011).
79. Wu, T. et al. A 16-channel nonparametric spike detection ASIC based on EC-PC decomposition. *IEEE Trans. Biomed. Circ. Syst.* **10**, 3–17 (2016).
80. Chen, T.-C., Chen, K., Yang, Z., Cockerham, K. & Liu, W. A biomedical multiprocessor SoC for closed-loop neuroprosthetic applications. In *IEEE Int. Solid-State Circuits Conference - Digest of Technical Papers* 434–435 (IEEE, 2009).
81. Karkare, V., Gibson, S. & Marković, D. A 75-μW, 16-channel neural spike-sorting processor with unsupervised clustering. *IEEE J. Solid-State Circ.* **48**, 2230–2238 (2013).
82. Do, A. T., Zeinolabedin, S. M. A., Jeon, D., Sylvester, D. & Kim, T. T.-H. An area-efficient 128-channel spike sorting processor for real-time neural recording with 0.175μW/channel in 65-nm CMOS. *IEEE Trans. VLSI Syst.* **27**, 126–137 (2018).
83. Aprile, C. et al. Adaptive learning-based compressive sampling for low-power wireless implants. *IEEE Trans. Circ. Syst. I* **65**, 3929–3941 (2018).
84. Ranjandish, R. & Schmid, A. A sub-μW/channel, 16-channel seizure detection and signal acquisition SoC based on multichannel compressive sensing. *IEEE Trans. Circ. Syst. II* **65**, 1400–1404 (2018).
85. Liu, X. et al. A fully integrated wireless compressed sensing neural signal acquisition system for chronic recording and brain machine interface. *IEEE Trans. Biomed. Circ. Syst.* **10**, 874–883 (2016).
86. Biederman, W. et al. A 4.78mm² fully-integrated neuromodulation SoC combining 64 acquisition channels with digital compression and simultaneous dual stimulation. *IEEE J. Solid-State Circ.* **50**, 1038–1047 (2015).
87. Kim, S.-J. et al. A sub-μW/Ch analog front-end for Δ-neural recording with spike-driven data compression. *IEEE Trans. Biomed. Circ. Syst*. https://doi.org/10.1109/TBCAS.2018.2880257 (2018).
88. Liu, X., Zhang, M., Richardson, A. G., Lucas, T. H. & Van der Spiegel, J. Design of a closed-loop, bidirectional brain machine interface system with energy efficient neural feature extraction and PID control. *IEEE Trans. Biomed. Circ. Syst.* **11**, 729–742 (2017).
89. Venkatraman, S., Elkabany, K., Long, J. D., Yao, Y. & Carmena, J. M. A system for neural recording and closed-loop intracortical microstimulation in awake rodents. *IEEE Trans. Biomed. Eng.* **56**, 15–22 (2009).
90. Mendrela, A. E. et al. A bidirectional neural interface circuit with active stimulation artifact cancellation and cross-channel common-mode noise suppression. *IEEE J. Solid-State Circ.* **51**, 955–965 (2016).
91. Zhou, A., Johnson, B. C. & Muller, R. Toward true closed-loop neuromodulation: artifact-free recording during stimulation. *Curr. Opin. Neurobiol.* **50**, 119–127 (2018).
92. Stanslaski, S. et al. Creating neural "co-processors" to explore treatments for neurological disorders. In *IEEE Int. Solid-State Circuits Conference (ISSCC)* 460–462 (IEEE, 2018).
93. Thomas, G. P. & Jobst, B. C. Critical review of the responsive neurostimulator system for epilepsy. *Med. Dev.* **8**, 405 (2015).
94. Kohler, F. et al. Closed-loop interaction with the cerebral cortex: a review of wireless implant technology. *Brain-Comp. Interf.* **4**, 146–154 (2017).
95. Xu, J. et al. A 160μW 8-channel active electrode system for EEG monitoring. *IEEE Trans. Biomed. Circ. Syst.* **5**, 555–567 (2011).
96. Xu, J. et al. A 665μW silicon photomultiplier-based NIRS/EEG/EIT monitoring ASIC for wearable functional brain imaging. In *IEEE Int. Solid-State Circuits Conference (ISSCC)* 294–296 (IEEE, 2018).
97. Pfurtscheller, G. et al. The hybrid BCI. *Front. Neurosci.* **4**, 30 (2010).
98. Schwarz, D. A. et al. Chronic, wireless recordings of large-scale brain activity in freely moving rhesus monkeys. *Nat. Methods* **11**, 670–676 (2014).
99. Angotzi, G. N., Boi, F., Zordan, S., Bonfanti, A. & Vato, A. A programmable closed-loop recording and stimulating wireless system for behaving small laboratory animals. *Sci. Rep.* **4**, 5963 (2014).
100. Yin, M. et al. Wireless neurosensor for full-spectrum electrophysiology recordings during free behavior. *Neuron* **84**, 1170–1182 (2014).
101. Zhou, A. et al. A wireless and artefact-free 128-channel neuromodulation device for closed-loop stimulation and recording in non-human primates. *Nat. Biomed. Eng.* **3**, 15–26 (2019).
102. Serruya, M. D., Hatsopoulos, N. G., Paninski, L., Fellows, M. R. & Donoghue, J. P. Brain-machine interface: Instant neural control of a movement signal. *Nature* **416**, 141–142 (2002).
103. Taylor, D. M., Tillery, S. I. H. & Schwartz, A. B. Direct cortical control of 3D neuroprosthetic devices. *Science* **296**, 1829–1832 (2002).
104. Wolpaw, J. R. & McFarland, D. J. Control of a two-dimensional movement signal by a noninvasive brain-computer interface in humans. *Proc. Natl Acad. Sci. USA* **101**, 17849–17854 (2004).
105. Rebsamen, B. et al. A brain controlled wheelchair to navigate in familiar environments. *IEEE Trans. Neural Syst. Rehabil. Eng.* **18**, 590–598 (2010).
106. Chaudhary, U., Birbaumer, N. & Ramos-Murguialday, A. Brain–computer interfaces for communication and rehabilitation. *Nat. Rev. Neurol.* **12**, 513–525 (2016).
107. Tran, N. et al. A complete 256-electrode retinal prosthesis chip. *IEEE J. Solid-State Circ.* **49**, 751–765 (2014).
108. Ramos-Murguialday, A. et al. Brain–machine interface in chronic stroke rehabilitation: a controlled study. *Ann. Neurol.* **74**, 100–108 (2013).
109. Capogrosso, M. et al. A brain–spine interface alleviating gait deficits after spinal cord injury in primates. *Nature* **539**, 284–288 (2016).
110. Wagner, F. B. et al. Targeted neurotechnology restores walking in humans with spinal cord injury. *Nature* **563**, 65–71 (2018).
111. Chortos, A., Liu, J. & Bao, Z. Pursuing prosthetic electronic skin. *Nat. Mater.* **15**, 937–950 (2016).
112. Tabot, G. A. et al. Restoring the sense of touch with a prosthetic hand through a brain interface. *Proc. Natl Acad. Sci. USA* 18279–18284 (2013).
113. Lopez, C. M. et al. 22.7 A 966-electrode neural probe with 384 configurable channels in 0.13 μm SOI CMOS. In *2016 IEEE Int. Solid-State Circuits Conference (ISSCC)* 392–393 (IEEE, 2016).

114. Herbawi, A. S., Kießner, L., Paul, O. & Rüther, P. High-density CMOS neural probe implementing a hierarchical addressing scheme for 1600 recording sites and 32 output channels. In *19th Int. Conf. Solid-State Sensors, Actuators and Microsystems (TRANSDUCERS)* 20–23 (IEEE, 2017).
115. De Dorigo, D. et al. A fully immersible deep-brain neural probe with modular architecture and a delta-sigma ADC integrated under each electrode for parallel readout of 144 recording sites. In *IEEE Int. Solid-State Circuits Conference (ISSCC)* 462–464 (IEEE, 2018).
116. Viventi, J. et al. Flexible, foldable, actively multiplexed, high-density electrode array for mapping brain activity in vivo. *Nat. Neurosci* **14**, 1599–1605 (2011).
117. Biederman, W. et al. A fully-integrated, miniaturized (0.125 mm^2) 10.5 μW wireless neural sensor. *IEEE J. Solid-State Circ.* **48**, 960–970 (2013).
118. Kim, C. et al. A 3 mm× 3 mm fully integrated wireless power receiver and neural interface system-on-chip. *IEEE Trans. Biomed. Circ. Syst.* **13**, 1736–1746 (2019).
119. Yeon, P., Bakir, M. S. & Ghovanloo, M. Towards a 1.1 mm^2 free-floating wireless implantable neural recording SoC. In *2018 IEEE Custom Integrated Circuits Conference (CICC)* https://doi.org/10.1109/CICC.2018.8357048 (IEEE, 2018).
120. Khalifa, A. et al. The microbead: A 0.009mm^3 implantable wireless neural stimulator. *IEEE Trans. Biomed. Circ. Syst.* **13**, 971–985 (2019).
121. Leung, V. W. et al. A CMOS distributed sensor system for high-density wireless neural implants for brain-machine interfaces. In *ESSCIRC 2018-IEEE 44th European Solid State Circuits Conference (ESSCIRC)* 230–233 (IEEE, 2018).
122. Jia, Y. et al. A mm-sized free-floating wirelessly powered implantable optical stimulating system-on-a-chip. In *IEEE Int. Solid-State Circuits Conference-(ISSCC)* 468–470 (IEEE, 2018).
123. Ghanbari, M. M. et al. 17.5 A 0.8 mm^3 ultrasonic implantable wireless neural recording system with linear AM backscattering. In *2019 IEEE Int. Solid-State Circuits Conference (ISSCC)* 284–286 (IEEE, 2019).
124. Charthad, J. et al. A mm-sized wireless implantable device for electrical stimulation of peripheral nerves. *IEEE Trans. Biomed. Circ. Syst.* **12**, 257–270 (2018).
125. Neely, R. M., Piech, D. K., Santacruz, S. R., Maharbiz, M. M. & Carmena, J. M. Recent advances in neural dust: towards a neural interface platform. *Curr. Opin. Neurobiol.* **50**, 64–71 (2018).
126. Leene, L. B. et al. Autonomous SoC for neural local field potential recording in mm-scale wireless implants. In *2018 IEEE Int. Symp. Circuits and Systems (ISCAS)* https://doi.org/10.1109/ISCAS.2018.8351147 (IEEE, 2018).
127. Laiwalla, F. et al. A distributed wireless network of implantable sub-mm cortical microstimulators for brain-computer interfaces. In *2019 41st Annu. Int. Conf. IEEE Engineering in Medicine and Biology Society (EMBC)* 6876–6879 (IEEE, 2019).
128. Naor, O., Krupa, S. & Shoham, S. Ultrasonic neuromodulation. *J. Neural Eng.* **13**, 031003 (2016).
129. Gagnon-Turcotte, G., Ethier, C., De Köninck, Y. & Gosselin, B. A 13μm CMOS SoC for simultaneous multichannel optogenetics and electrophysiological brain recording. In *2018 IEEE Int. Solid-State Circuits Conference (ISSCC)* 466–468 (IEEE, 2018).
130. Boyden, E. S., Zhang, F., Bamberg, E., Nagel, G. & Deisseroth, K. Millisecond-timescale, genetically targeted optical control of neural activity. *Nat. Neurosci.* **8**, 1263–1268 (2005).
131. Deisseroth, K. Optogenetics: 10 years of microbial opsins in neuroscience. *Nat. Neurosci.* **18**, 1213–1225 (2015).
132. Ding, H. et al. Microscale optoelectronic infrared-to-visible upconversion devices and their use as injectable light sources. *Proc. Natl Acad. Sci. USA* **115**, 6632–6637 (2018).
133. Anikeeva, P. et al. Optetrode: a multichannel readout for optogenetic control in freely moving mice. *Nat. Neurosci.* **15**, 163–170 (2012).
134. Kim, T.-i et al. Injectable, cellular-scale optoelectronics with applications for wireless optogenetics. *Science* **340**, 211–216 (2013).
135. Hodgkin, A. Evidence for electrical transmission in nerve. *J. Physiol.* **90**, 183–210 (1937).

Acknowledgements

This work is supported in part by the Beijing Innovation Center for Future chip, in part by the Beijing National Research Center for Information Science and Technology, in part by the Natural Science Foundation of China through grant 61674095.

Author contributions

M.Z. and J.V.d.S. conceived the work and suggested the outline of the paper. M.Z. and X.L. worked on the study of various neural interface designs. Z.T. and M.Z. carried out investigations and wrote the paper.

Competing interests

The authors declare no competing interests.

Additional information

Correspondence should be addressed to M.Z.